Transformation Hardening of Steel Using High-Energy Electron Beams

The high-energy electron beam process can heat treat steel to depths not attainable with other processes

BY J. W. ELMER, M. A. NEWTON and A. C. SMITH, JR.

ABSTRACT. Megavolt/megawatt high-energy electron beams (HEEBs) represent a new generation of charged particle beams that have unique capabilities for advanced processing of materials. These beams have energies in the 1 to 10 MeV range, which enables them to deposit energy volumetrically within the material being processed, under rapid and controlled conditions. One material processing application for HEEBs is the localized transformation hardening of steel. The high accelerating voltage of the electron beam allows its energy to be deposited subsurface, so that the steel can be heat treated at depth without melting, while the beam's high average power allows transformation hardening to be performed at rapid surface coverage rates. In this investigation, a 6 MeV electron beam was used to process plain carbon steel and O-1 tool steel using stationary and traveling beams, at normal and glancing angles of incidence. These experiments investigated the beam fluence thresholds for transformation hardening, melting, and vaporization of steel. Localized transformation hardening of steel was performed at a surface fluence of approximately 20 J/mm^2, which hardened the steel to a depth of nearly 2 mm without melting, thus producing a microstructure that was free of solidification-related defects such as cracking and porosity. Achieving deep localized heat treating of steel to its peak hardness without surface melting and at high surface coverage rates is not possible by conventional directed energy beam processing techniques.

J. W. ELMER and M. A. NEWTON are with Lawrence Livermore National Laboratory, Livermore, Calif. A. C. SMITH, JR., is with Ballena Systems Corp.

Paper presented at the 74th Annual AWS Meeting, held April 25–29, 1993, in Houston, Tex.

Introduction

Localized heat treating of steel requires the steel to first be austenitized for sufficient time to dissolve, or partially dissolve, the carbides present in the microstructure, and then the steel must be rapidly cooled in order to harden the steel through the formation of martensite. Austenitizing the steel places low- and high-temperature limits on the heat treating process if melting is to be avoided, and transformation hardening of this microstructure requires a high cooling rate in order to form martensite. Conventional methods for localized hardening of steel such as laser and electron beam processing heat only the surface of the steel. For example, energy absorption ranges are on the order of 10 μm for 100 kV electrons and less than 1 μm for photons. Heating with these beams occurs by thermal conduction from the surface of the material only since no internal energy is deposited by the heat source. Therefore, the conduction of heat by thermal diffusion places limitations on the maximum depth to which a steel can be fully hardened by conventional localized heat sources. Typically, localized heat treating by conventional beam processing is limited to approximately 1 mm (0.04 in.) maximum depth (Refs. 1, 2).

KEY WORDS

High-Energy EB
Electron Beam
Transform. Hardening
Vaporiz. Threshold
Localized Heating
Incidence Angles
Coverage Rates
Rapid Thermal Proc.
Volumetric Heating

High-energy electron beams differ from conventional electron beams in that they deposit energy deeply and rapidly into the material being processed. The range over which the electrons interact with the material depends on the kinetic energy of the beam and the properties of the material being processed. Monte Carlo simulations of the energy deposition by HEEBs indicate that the electron range is on the order of 1 cm for steel (Ref. 3), and that scattering of the electrons from within the steel leads to a maximum energy deposition approximately 1 mm below the surface of the plate. Thus, the deeply penetrating HEEB electrons can austenitize the steel at depth, while the rapid self quenching of the short-duration heat pulse can transformation harden this zone without immersion into a quenching medium (Ref. 4).

In this investigation, a 6-MeV electron beam was used to process mild steel and tool steel for the purpose of gaining a fundamental understanding of deep localized transformation hardening of steel with HEEBs. Experiments were performed on steel plates by rapidly heating the steel to peak temperatures near its melting point using both stationary and moving HEEBs. Results from these experiments confirm the Monte Carlo calculations of the energy deposition in steel, and demonstrate that a deep and nearly uniform transformation hardened zone

Fig. 1 — Schematic drawing of the materials processing section of the ETA II accelerator. The 6-MeV beam enters from the right-hand side of the figure, and separate magnets are used for positioning/scanning and focusing the beam on the workpiece.

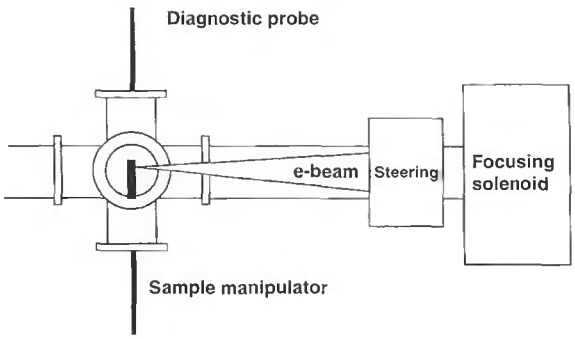

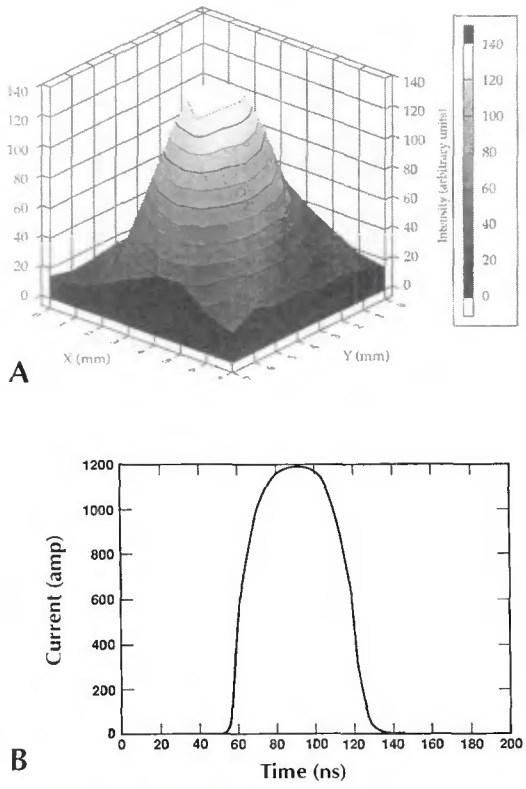

Fig. 2 — A — Surface plot of the electron distribution in a 1 kA/pulse, 6 MeV beam from a digitized image produced by a quartz thin-foil diagnostic; B — current vs. time plot of the pulse width from a 1-kA/pulse, 6-MeV beam.

can be produced in steel at rapid surface coverage rates. In addition, high fluence experiments were conducted on steel to determine the melting and vaporization thresholds for this beam.

Experimental Procedures

Electron Accelerator

The experimental test accelerator II (ETA II) at Lawrence Livermore National Laboratory is a linear induction accelerator capable of producing up to 50 pulses of a 2.5-kA electron beam at peak pulse repetition rates of 2 kHz. The pulse duration is approximately 60 ns full width half maximum (FWHM), giving several hundred joules of energy per pulse. This facility combines high-brightness (~100 A/[mm-rad]^2), high-electron beam currents (2.5 kA maximum) and energies in excess of 5 MeV with high average power capability (~2 MW maximum). The high brightness of ETA II enables the beam to be focused to a spot diameter of approximately 3.5 mm, which corresponds to a beam power density on the workpiece of up to ~20 MW/cm^2 averaged over a burst of 50 pulses. The focused beam can be precisely controlled using a magnetic beam steering system to position the beam at specific locations on the workpiece or to rapidly scan the beam across the surface of the workpiece. The total number of pulses and the repetition rate can also be easily varied to tailor the magnitude and rate of energy deposition into the workpiece.

Materials processing experiments were conducted at the end of the ETA II accelerator in an evacuated cavity with viewing ports to monitor the experiments, as illustrated in Fig. 1. The size and position of the electron beam were determined using a charged coupled device camera to image the optical Cerenkov radiation emitted from a thin quartz foil placed in the beam path (Ref. 5). Once the beam was properly positioned and characterized, the quartz foil was removed and the workpiece was inserted into the path of the electron beam. A surface contour plot of the electron distribution in a tightly focused beam is shown in Fig. 2A, indicating that the beam can be focused to a diameter as small as 3.5 mm (0.14 in.) FWHM.

All experiments in this investigation were performed using a 6-MeV electron beam with a vacuum of 10^{-6} torr at the workpiece location. The electron beam pulse duration was maintained constant at 60 ns FWHM for all experiments, and a typical current vs. time profile is shown in Fig. 2B. The pulse repetition frequency (PRF), defined as the frequency at which the pulses are delivered in each burst, was adjusted between 100 and 2000 Hz, and the beam current was adjusted between 0.9 and 1.25 kA/pulse, thus providing approximately 325 to 450 J/pulse. Machine operation was limited to 50 pulses in a single burst, however, bursts could be repeated approximately every minute.

Materials Processing and Characterization

Materials processing experiments were performed by placing 5- and 25-mm (0.2- and 1-in.) thick by 100-mm (4-in.) square plates in the beam line of the ETA II accelerator and processing the plates with various fluences at an acceleration voltage of 6 MeV. Experiments were first conducted on cold finished AISI 1018 plain carbon steel (0.16%C, 0.68%Mn, 0.12%Cr, 0.25%Si) to study the basic interaction of the HEEBs with the steel plate. The effects of the beam's average power, power density, energy density, and the total energy deposited per unit area were investigated by varying the PRF, beam diameter, travel speed and number of pulses per burst. Results from these experiments were then used to guide localized heat treating experiments on 12 x 50 x 100-mm (0.5 x 2 x 4-in.) plates of an oil hardening O-1 tool steel (0.94%C, 1.20%Mn, 0.5%Cr, 0.5%W, 0.3%Si).

Stationary electron beams were used to produce up to nine surface-treated

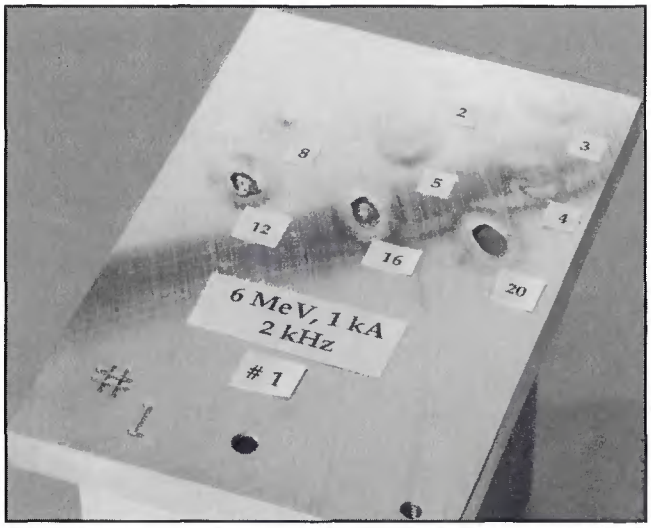

Fig. 3 — Plain carbon steel plate (100 x 100 x 5 mm) processed using a 5-mm-diameter, 6-MeV, 1-kA/pulse beam operating at 2 kHz PRF. The number of pulses per spot are indicated on the 5-mm-thick plate.

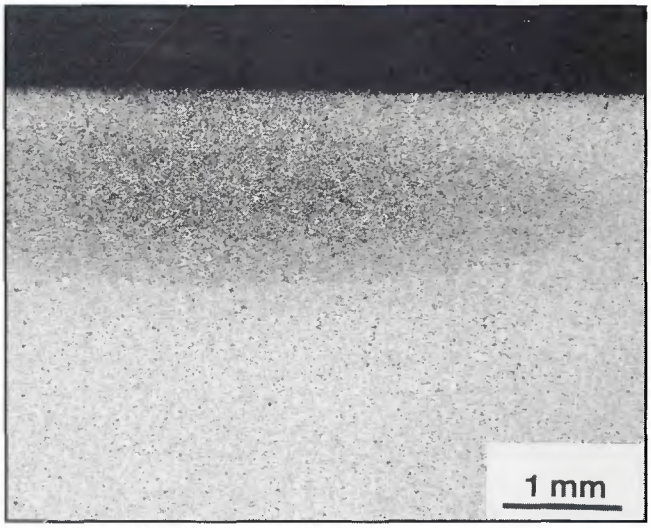

Fig. 4 — A subsurface heat-treated zone in plain carbon steel produced at a fluence of 21 J/mm^2 produced by 6 pulses from a 10-mm-diameter beam.

spots on each steel plate by magnetically steering the beam to a new location on the plate prior to each experiment. Moving electron beams were used to heat treat strips of material by magnetically scanning the beam at speeds up to 0.4 m/s (1.3 ft/s) across the surface of the plate. The moving beams produced a series of 50 overlapping pulses per run, which heat treated a strip approximately 10 mm wide by 50 mm long (0.4 x 2 in.). The test coupons were held in the beam line on a retractable sample holder, which allowed the quartz diagnostic probe to periodically be inserted into the beam line at the same location as the test sample in order to measure the position and diameter of the beam. In addition, the sample holder could be rotated up to 180 deg to allow the beam to interact with the test coupon at glancing angles.

Specimens processed by the HEEBs were analyzed using optical microscopy, transmission electron microscopy (TEM), and microhardness measurements. Optical microscopy was performed by cutting cross-sectional slices through the center of stationary spot processed regions, and by cutting cross-sectional slices through heat treated strips produced by moving beams. Conventional metallographic procedures were used to polish these samples in preparation for etching in a 4% HNO_3 - ethyl alcohol mixture (nital). Transmission electron microscopy was performed using a JEOL 200CX microscope. Thin foil specimens were prepared for TEM analysis by electropolishing in an acetic acid-10% perchloric electrolyte at 20 volts, prior to uniformly thinning the polished region using an ion milling technique. Vickers microhardness (DPH) measurements were made by traversing down the centerline of the heat treated regions, using a diamond pyramid indentor and a 100-g load. Hardness conversions from DPH to Rockwell C (Rc) were made using the relationship $Rc = -35.1 + 0.304\ DPH - 0.341 \times 10^{-3}\ DPH^2 + 0.145 \times 10^{-6}\ DPH^3$, which is a third-order fit to the hardness conversion table published by ASM International (Ref. 6).

Results and Discussion

Phase Transformation Thresholds in Plain Carbon Steel

The interaction of the 6-MeV electron beam with plain carbon steel was studied in order to determine the beam fluence thresholds for annealing/hardening, melting and vaporization. Experiments were conducted to investigate the effects of beam fluence (energy deposited per unit surface area) on the microstructure of the steel. Both the diameter of the beam and the number of pulses incident on a given spot were used to produce variations in beam fluence from 10 to 150 J/mm^2.

Figure 3 shows a photograph of a steel plate that was processed with a 6-mm (0.24-in.) diameter beam at eight different locations. Each location received a different number of pulses at a 2-kHz pulse repetition frequency (PRF). At five pulses or less, the plate showed no significant signs of surface damage other than discoloration and a slight rippling of the surface on the edge of the beam interaction area. At eight pulses, the plate began to swell, creating a small dimple on the surface of the plate near the center of the beam interaction area. At twelve or more pulses, the plate developed a crater, as the beam drilled into the steel. Metallographic cross-sections through the processed regions of the plain carbon steel plate were prepared to examine the modifications to the steel.

Heat treating was performed using a an average fluence of 21 J/mm^2 on the surface of the steel plate. Figure 4 shows a metallographic cross-section through one of the heat treated samples that was processed with 6 pulses from a 10-mm diameter, 6-MeV, 0.9-kA/pulse beam operating at 2 kHz PRF. No melting was observed in this sample, and the heat treated region, which etches darker than the base material, is elliptical in cross-section and is centered below the surface of the plate. This unique shape of the heat treated region indicates that the beam internally heated the steel, and the center of the heat treated region is located 1-mm below the surface of the plate. The diameter of the heat treated region is approximately 9 mm (0.36 in.), which is

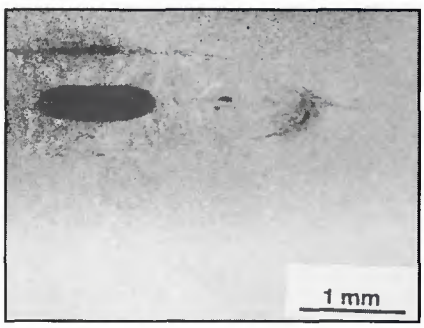

Fig. 5 — A subsurface resolidified nugget and small void in plain carbon steel produced at a fluence of 95 J/mm^2 with 10 pulses from a 6-mm diameter beam.

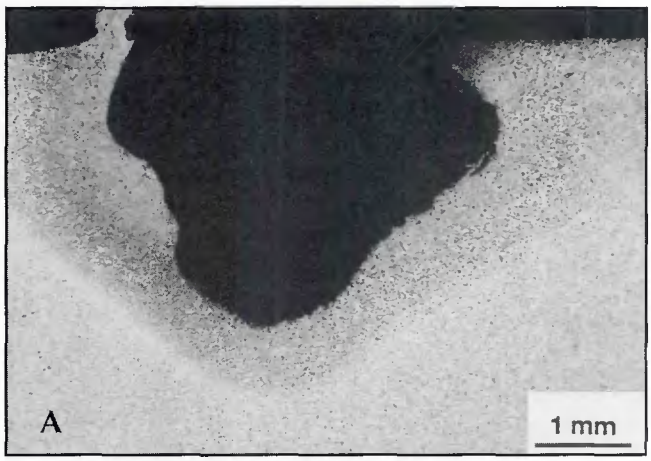

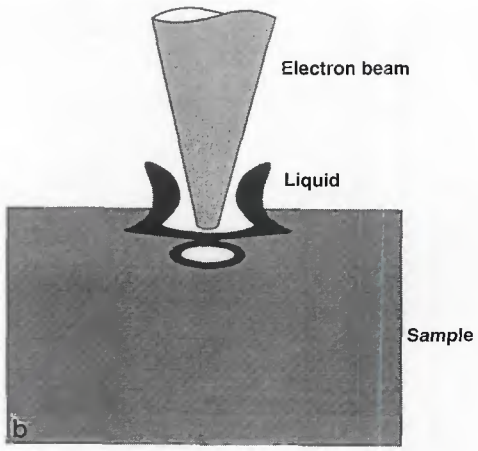

Fig. 6 — A — A 4-mm deep cavity produced in plain carbon steel at a fluence of 140 J/mm2 with 5 pulses from a 3.5 mm diameter beam; B — Schematic drawing of the initial stages of drilling with HEEBs, illustrating liquid expulsion from the first cavity and the formation of a second, smaller, subsurface cavity.

similar to the diameter of the beam, and there exists evidence of heat treating to a depth of approximately 2 mm (0.08 in.) below the surface of the plate.

Subsurface melting and vaporization occurred at fluences on the order of 100 J/mm^2. Figure 5 shows a metallographic cross-section through a region of a steel plate that was processed with 10 pulses from a 6-mm diameter, 6-MeV, 0.9-kA/pulse beam operating at 2 kHz PRF, at an average fluence of 95 J/mm^2. This plate showed signs of surface swelling, and a metallographic cross-section was taken through the center of the dimple that appeared on the surface of the plate. This cross-section revealed the presence of a molten zone and a small subsurface void, which formed when the internal pressure within the vapor cavity expanded the steel and deformed the surface of the plate outward.

Drilling occurred at higher fluences. Figure 6A shows a metallographic cross-section through a crater that was drilled with five pulses from a 3.5-mm (0.14 in.) diameter, 6-MeV, 0.9-kA/pulse beam operating at 500 Hz PRF. These conditions led to a fluence of 140 J/mm^2, which was sufficiently high to vaporize the steel and drill into the plate to a depth of approximately 4 mm (0.16 in.). The drilling appeared to occur in two stages, leaving a two-tiered crater. The upper tier of the crater has the approximate dimensions as one would expect from the location and size of the subsurface nugget observed at lower fluences, while the lower tier of the crater is smaller in diameter. This interaction is illustrated in Fig. 6B, which schematically shows the creation of two successive subsurface voids that erupted to form the observed crater.

Further experiments were conducted on plain carbon steel at higher fluences in order to determine the drilling rate of HEEBs into steel. Figure 7 plots the results of these experiments, showing the crater depth as a function of total number of pulses for a 5-mm (0.2-in.) diameter, 1.0-kA, 6-MeV beam, operating at two different PRFs of 100 and 2000 Hz. This figure shows that the crater depth increases to approximately 8 mm (0.31 in.) at 50 pulses, and that the drilling rate is higher at the higher PRF. The width of the crater is approximately the same as the beam diameter at low numbers of pulses, however, the width of the opening becomes larger with increasing number of pulses. At 50 pulses, the width of the crater was measured to be approximately twice the diameter of the beam at the surface of the plate, but narrowed down to less than 1 mm near the bottom of the crater.

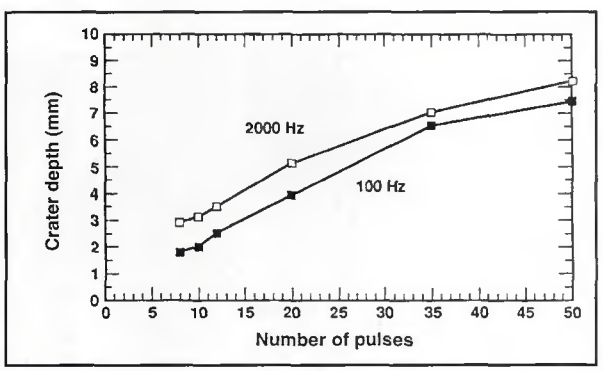

Fig. 7 — Crater depth in plain carbon steel as a function of the number of pulses at PRFs of 100 and 2000 Hz, for a 6-MeV, 1-kA/pulse, 5-mm diameter beam.

Results from these high fluence experiments indicate that the initial stage of drilling occurred by a discontinuous process whereby subsurface heating and eruption occur periodically as the beam drilled into the steel. However, as the crater became deeper, the beam's energy became spread out over the increased surface area of the crater. This reduction in energy per unit area of the crater wall reduced the amount of subsurface vaporization and reduced the amount of large scale violent eruptions that occurred. Eventually, a deep conical crater developed that narrowed to a point, as shown in Fig. 8. This radiograph shows a deep hole that was drilled into a 25-mm wide x 75-mm (1 x 3 in.) thick plain carbon steel plate using 10 bursts of 50 pulses (500 total pulses) with a 4-mm-diameter, 6-MeV, 1.2-kA beam operating at 2000 Hz PRF. Figure 8A shows a top view of the hole down the axis of the beam, indicating that the hole has an elliptical cross-section with a major axis width of 15 mm and a minor axis width of 10 mm at the top surface of the plate. Figure 8B shows a side view of this hole, which penetrates into the steel to a depth of approximately 60 mm (2.4 in.) and narrows down to less than 1 mm in diameter at the bottom of the hole.

Therefore, for stationary spot-processed regions of steel, the results of these experiments showed that localized transformation hardening to approximately 2-mm depth can be performed with a 6-MeV beam at a fluence of 21

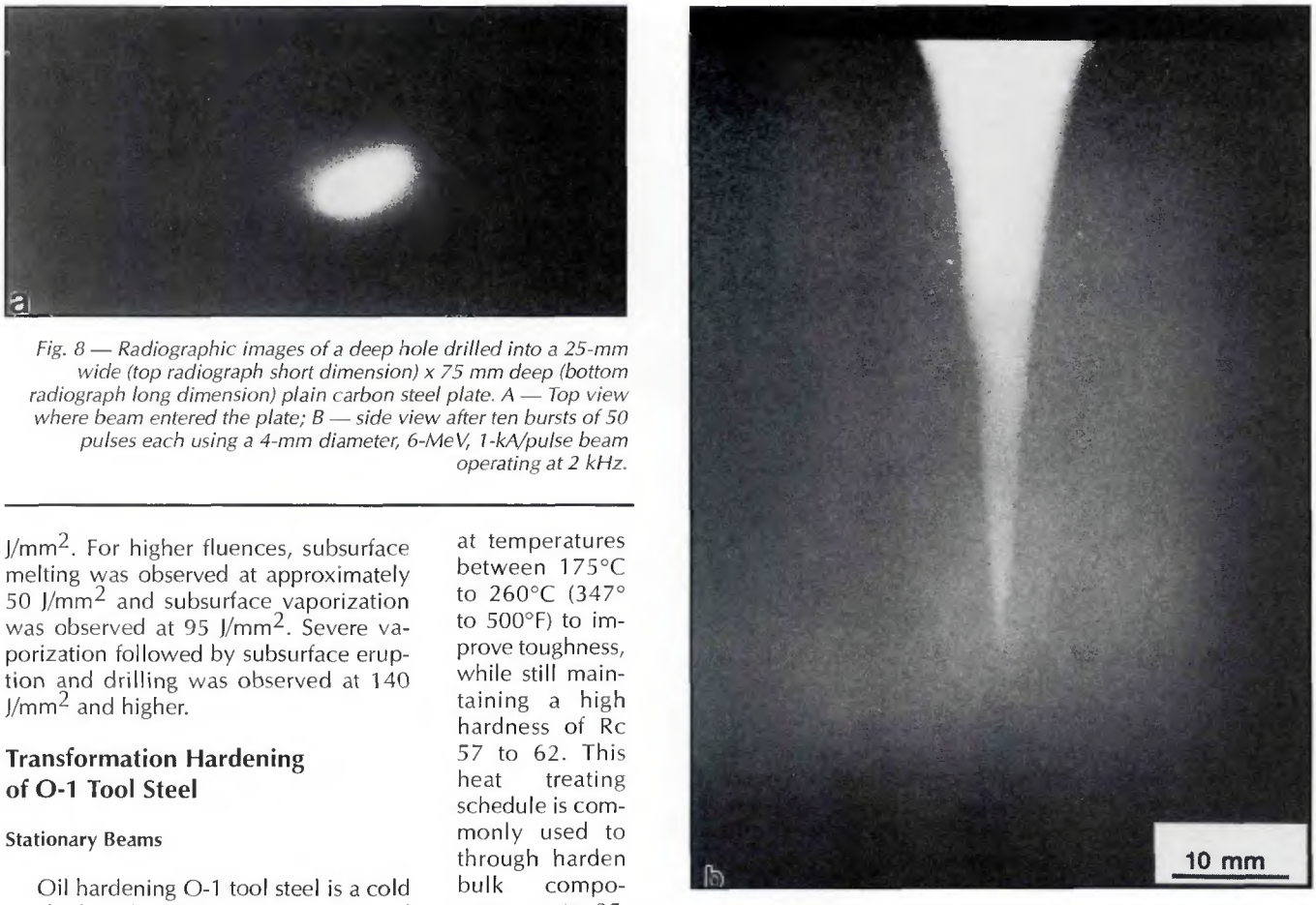

Fig. 8 — Radiographic images of a deep hole drilled into a 25-mm wide (top radiograph short dimension) x 75 mm deep (bottom radiograph long dimension) plain carbon steel plate. A — Top view where beam entered the plate; B — side view after ten bursts of 50 pulses each using a 4-mm diameter, 6-MeV, 1-kA/pulse beam operating at 2 kHz.

J/mm^2. For higher fluences, subsurface melting was observed at approximately 50 J/mm^2 and subsurface vaporization was observed at 95 J/mm^2. Severe vaporization followed by subsurface eruption and drilling was observed at 140 J/mm^2 and higher.

Transformation Hardening of O-1 Tool Steel

Stationary Beams

Oil hardening O-1 tool steel is a cold worked tool and die steel with good hardenibility, moderate toughness, and good dimensional stability on quenching (Ref. 7). Prior to hardening, the annealed microstructure consists of micron-sized spheroidal carbides in a ferrite matrix; after transformation hardening, the microstructure consists of similar carbide particles in a martensitic matrix with some retained austenite. This steel is typically heat treated by solution heating to temperatures between 760°C to 870°C (1400° to 1598°F) for 10 to 30 min., then quenching in oil to a hardness of Rc 63 to 65. Tempering may then be performed at temperatures between 175°C to 260°C (347° to 500°F) to improve toughness, while still maintaining a high hardness of Rc 57 to 62. This heat treating schedule is commonly used to through harden bulk components up to 25-mm thick.

Localized heat treating of O-1 tool steel was performed using the 6-MeV beam from the ETA II accelerator to harden the steel by individually heat treating discrete regions of the plate. Stationary beams and moving beams were used to rapidly heat and austenitize the steel at temperatures below its melting point, while transformation hardening occurred by self quenching into the steel substrate.

Figure 9 shows an optical metallographic cross-section of a HEEB processed region of the O-1 tool steel plate. This sample was processed using a fluence of 59 J/mm^2 with a stationary 9-mm-diameter, 6-MeV, 1.25-kA/pulse beam operating at 500 Hz PRF. Figure 9A shows a cross-section through the center of the processed region, indicating the presence of a subsurface void and solidification cracking around a subsurface molten zone. Figure 9B shows a cross-section through this same sample that was taken at a location approximately 4 mm off the center of the sample, which is

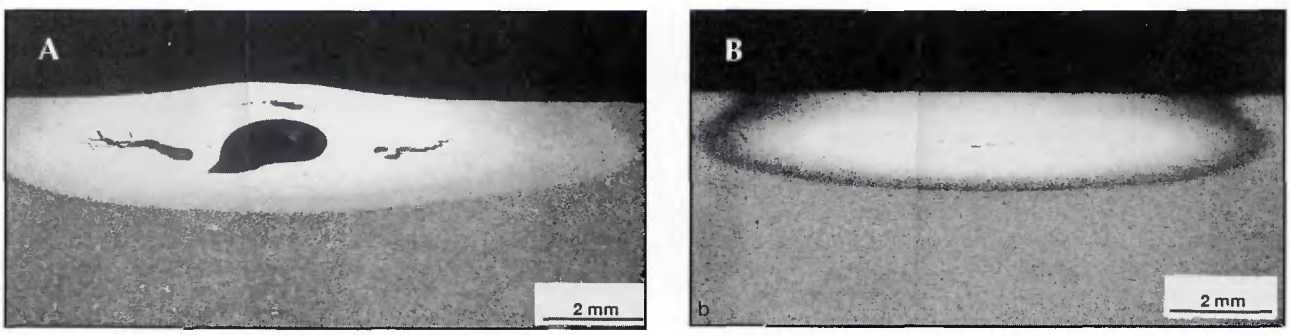

Fig. 9 — Transformation hardened O-1 tool steel produced at a fluence of 59 J/mm^2 with 10 pulses from a stationary 9-mm-diameter, 6-MeV, 1.25-kA/pulse beam operating at 500 Hz PRF. A — The microstructure through the center of the processed region; B — the microstructure through a section taken 4 mm out from the center of the processed region.

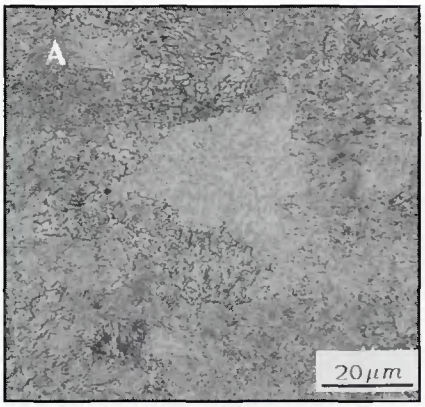

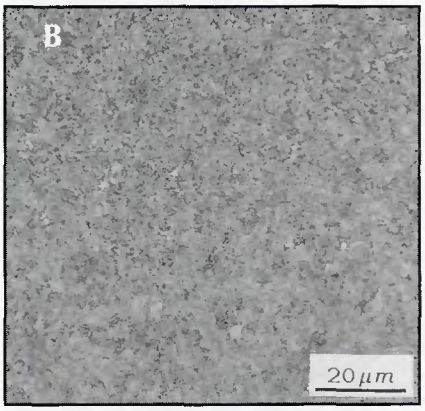

Fig. 10 — Optical micrographs of O-1 tool steel etched in nital. A — The as-received microstructure; B — the transformation hardened microstructure after 10 pulses from a stationary 9-mm-diameter, 6-MeV, 1.25-kA/pulse beam operating at 500 Hz PRF.

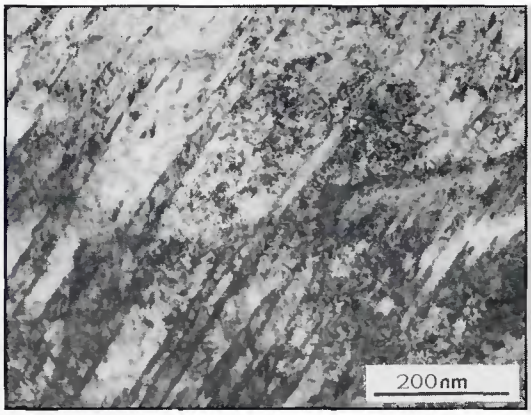

Fig. 11 — Transmission electron micrograph of the transformation hardened O-1 tool steel showing fine twins within a plate-type martensitic microstructure.

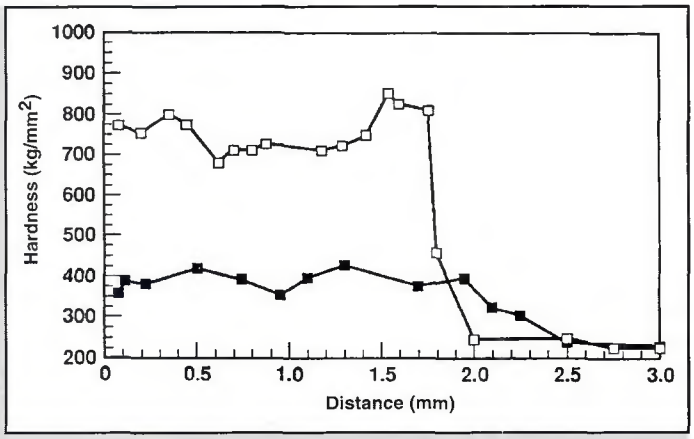

Fig. 12 — Microhardness comparison of transformation hardened O-1 tool steel and plain carbon steel. Measurements were taken from spot processed regions produced by stationary 9-mm-diameter, 6-MeV, 1.25-kA/pulse beams operating at 500 Hz PRF. The distance along the x-axis refers to depth into the steel plate.

just outside the molten region.

At high magnification, the microstructure of the tool steel is shown in Fig. 10A before processing and in Fig. 10B after processing. Prior to processing, the optical light micrograph shows that the microstructure consists of colonies of spheroidal carbide particles in a ferrite matrix, while after processing, the carbide particles are in a martensitic matrix and appear to have been slightly refined. The martensitic transformation hardened steel is shown in Fig. 11 at an even higher magnification using TEM. The transformed microstructure consists of a series of fine twins within a plate-type martensitic structure, which is characteristic of transformation hardened high-carbon steel.

The microhardness of the HEEB transformation hardened 0.94%C O-1 tool steel is shown in Fig. 12. In this plot, a microhardness traverse was made from the surface (distance = 0) and down the centerline of the hardened region shown in Fig. 9B. A similar plot for HEEB processed plain carbon steel is shown in this figure for comparison. The hardness of the tool steel is relatively uniform throughout the processed region to a depth of approximately 1.75 mm, with a slightly higher hardness near the surface of the plate and also near the base-metal/heat-treated zone boundary. The bulk of the processed region has a Vickers DPH hardness of 700 to 800 kg/mm^2 (Rc 60 to 64), which is a factor of 3 to 4 times greater than the hardness of the untreated base material (DPH 220). These hardness values are similar to the reported peak hardened condition of O-1 tool steel, which oil-quenches to a hardness of Rc 63 to 65 (Refs. 7, 8). The plain carbon steel also responded favorably to the localized heat treating process by forming a 2-mm-deep heat treated zone with a DPH hardness of 400 kg/mm^2 (Rc 41) throughout the bulk of the processed region. This represents a 2X increase in the hardness over that of the untreated base material, and is at the maximum hardness of 0.16%C steel (Ref. 8).

One advantage for transformation hardening with HEEBs is that heat can be deposited deeply into the material without melting the surface even though severe overheating may occur below the surface. For example, Fig. 13 compares scanning electron microscope images of the surface of the as-received steel and the HEEB transformation hardened steel directly above a subsurface resolidified region and void produced at a fluence of 59 J/mm^2. In both cases, the original machining marks are present on the surface of the steel plate, even though subsurface melting had occurred. Therefore, HEEB processing has little effect on the macroscopic characteristics of the surface of the plate even under extreme processing conditions. This allows tool and die components to be locally heat treated after final machining operations have been performed.

Moving Beams

Heat treating of certain components may favor a moving beam rather than a stationary beam to produce strips of heat treated material rather than spots of heat treated material. These conditions were

investigated in this study by scanning the electron beam across the surface of the O-1 tool steel plate at a speed of 0.4 m/s at 90- and 30-deg angles of incidence to the surface of the plate. This processing was performed using a 5-mm-diameter, 6-MeV, 0.9-kA/pulse beam operating for 50 pulses at a PRF of 500 Hz. These conditions led to an average surface fluence of 68 J/mm^2 along the strip. At this fluence no subsurface melting was observed, indicating that moving beams can tolerate a higher surface fluence than stationary beams before melting occurs in the substrate.

Figure 14A shows a metallographic cross-section through the tool steel that was processed at an angle of incidence of 90 deg, while Fig. 14B shows a similar view through the tool steel that was processed at an angle of incidence of 30 deg. At a 90-deg angle of incidence, the heat treated region measures about 7 mm wide and 2 mm deep, with an approximate rectangular cross-sectional shape. At a 30-deg angle of incidence the heat treated region measures approximately 7 mm wide and 1 mm deep, with a semi-elliptical cross-sectional shape. The reduced penetration of the beam at the glancing angle corresponds directly to a geometric effect, whereby the depth of electron penetration normal to the surface of the plate is proportional to the sine of the angle of incidence. It is important to note that the beam coupled very well with the tool steel at the glancing angle, since many components that require heat treating have curved or angled surfaces, such as gears and turbine blades. The ability of HEEBs to couple well with materials at glancing angles is advantageous, since high-power lasers, which are often used for localized heat treating of steels, do not couple well with materials at these angles.

Hardness measurements were made through the strips of heat treated tool steel that had been processed at both 90- and 30-deg angles of incidence. Figure 15 plots the results of these measurements, showing that the depth of hardening is approximately 1.8 mm for the 90-deg angle of incidence and 0.9 mm for the 30-deg angle of incidence. At the 90-deg angle of incidence, the hardness is relatively uniform between 750 and 800 kg/mm^2 (Rc 62 to 64) throughout the bulk of the heat treated zone. This is consistent with, but slightly harder than, the spot processed tool steel. The hardness near the surface of the plate is even greater than that in the bulk and reaches 940 kg/mm^2 (Rc 69.8). At the 30-deg angle of incidence, the hardness is less uniform throughout the processed region, with a hardness peak occurring approximately 0.6 mm below the surface of the plate at approximately 850 kg/mm^2 (Rc 66). Therefore, HEEBs are able to harden the O-1 tool steel to its maximum hardness in a localized manner at high surface coverage rates and at glancing angles.

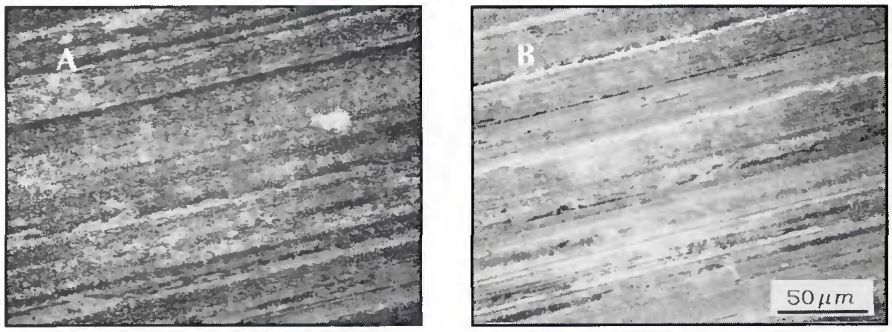

Fig. 13 — SEM micrographs of the surface of O-1 tool steel in: A — the as-received condition and B — HEEB transformation hardened condition. Results show that the HEEB treatment does not significantly alter the surface even though melting and vaporization occurred below the surface of the plate.

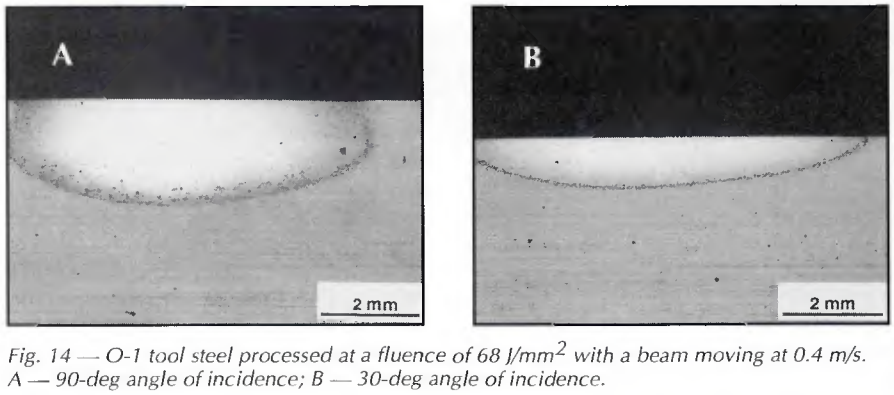

Fig. 14 — O-1 tool steel processed at a fluence of 68 J/mm^2 with a beam moving at 0.4 m/s. A — 90-deg angle of incidence; B — 30-deg angle of incidence.

Hardening depths up to 2.5 mm (0.1 in.) below the surface of the plate might be achieved with HEEBs in O-1 tool steel by tailoring the beam to produce steeper thermal gradients. Further increase in the hardening depth could also be achieved by increasing the kinetic energy of the high-energy electron beam to 10 MeV, where we might expect that steels could be fully hardened to depths up to 4 mm. Additional advantages for surface hardening with high-energy electron beams are the rapid processing rates (one to two orders of magnitude higher than with conventional high-power CO_2 lasers), the wide area that can be covered while still maintaining steep thermal gradients, the possibility of out-of-vacuum electron beam processing (Ref. 3), the ability to heat treat at glancing angles, and the favorable cross-sectional shape of the subsurface heat treated region (nearly rectangular for moving beams at a 90-deg angle of incidence) that allows efficient coverage with minimal overlapping of adjacent heat treated regions.

Monte Carlo Modeling of Energy Deposition

Modeling of the HEEB energy deposition in materials was performed using the CYLTRAN Monte Carlo transport code (Ref. 9). This code calculates the development of the electron/photon cascade that occurs as high-energy electrons enter and interact with the material. By following the three-dimensional particle trajectory of 2 x 10^4 electron histories into an axisymmetric workpiece, enough statistics are gathered to determine the spatial deposition of the beam's energy in J/g of material. Provisions are made in the code to input the composition of the workpiece and to simulate the effects of different beam radii, locations, and angles of impingement. The energy distribution is presently assumed to be uniform over the diameter of the beam, which models the beam/material interaction with sufficient accuracy for this investigation. However, modeling the beam with Gaussian energy distribution would provide a more realistic representation of the beam/material interaction and can be performed if increased accuracy is required.

Figure 16 shows the results of one

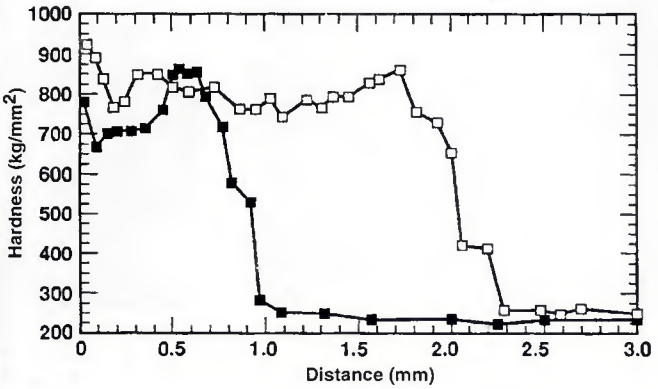

Fig. 15 — Microhardness measurements down the centerline of transformation hardened O-1 tool steel processed at 90- deg angle and 30-deg angles of incidence as shown in the previous figure.

Monte Carlo calculation that simulates the energy deposition in steel processed with a single pulse from a 9-mm-diameter, 6-MeV, 50-ns, 1.25-kA/pulse beam. The results show the iso-dose contours in J/g plotted as a function of radial distance from the beam axis. The energy dose reaches a maximum value of 275 J/g at a location approximately 1.3 mm below the surface of the plate, and drops off to a value of 25 J/g at approximately 4 mm below the surface of the plate. The diameter of the energy-dosed region is approximately 10 mm at the surface of the plate, which is similar to the diameter of the beam, and the diameter of the dosed region expands to approximately 12 mm at a depth of 1.5 mm below the surface of the plate. These calculations are a simulation of the experimental results shown in Fig. 9A, which is a metallographic cross-section through the center of the O-1 tool steel sample that was processed with 10 pulses of the same parameters. Qualitatively, the diameter of the processed region, cross-sectional shape, and depth of maximum heating all show a close similarity to the iso-dose contours predicted by the model.

Quantitative analysis and comparison of the Monte Carlo code with the experimental results from the ETA II tests can be made by assuming that an insignificant amount of heat diffusion occurs throughout the duration of the 10 pulses at 500 Hz PRF (200 ms). This assumption allows the total energy dose to be estimated by the number of pulses times the energy dose per pulse, and can be made because the heat will only diffuse about 1 mm during the time the first and last pulses enter the sample, as estimated from $x^2 = 4\ \alpha t$, where x is the diffusion distance and t is the diffusion time. The thermal diffusivity, α, was determined from the relationship $\alpha = k/(\rho C_p)$ where C_p is the heat capacity, k is the thermal conductivity, and ρ is the density of the steel — Table 1.

The temperature rise in the steel is related to the energy dose, the heat capacity of the steel, and the enthalpy of any phase transitions that occur. Phase transition enthalpies, $\Delta H_{\alpha\text{-}\gamma}$, $\Delta H_{\gamma\text{-}L}$, and $\Delta H_{L\text{-}V}$, correspond to the bcc-to-fcc, fcc-to-liquid, and liquid-to-vapor, phase transitions, respectively, are summarized in Table 1 (Ref. 10), while the coefficients, a and b, of the temperature-dependent heat capacity ($C_P(T)$) of these phases are given in Table 2 for the relationship $C_P(T) = a + bT$ (Ref. 11). Within a given phase, the temperature-dose relationship was determined using the following equation:

$$D = \int_{To}^{T_f} C_p(T)\,dT$$

where D is the dose given to the sample, T is the temperature, To is the initial temperature, and T_f is the final temperature after processing. The enthalpy of transformation is further added to the required dose at each of the phase transformation temperatures.

These data were used to calculate the dose required to form austenite, liquid, or vapor, and the results are summarized in Table 3, where T_{A3} (800°C), T_L (1475°C) and T_V (2730°C) correspond to the austenite, melting, and vaporization temperatures of the 0.94%C steel, respectively. Table 3 indicates that the dose required to heat and transform the steel to austenite is 575 J/g, the dose to melt the steel is 1207 J/g, and the dose to vaporize the steel is 8195 J/g.

The HEEB processed tool steel shown in Fig. 9A received ten individual pulses, which corresponds to a maximum calculated dose of 2750 J/g directly below the beam as estimated from the Monte Carlo calculation. This energy dose would be sufficient to exceed the vaporization temperature and partially vaporize the processed region. Figure 9A shows the results of the experiment, and indicates that subsurface melting and vaporization did indeed occur after ten pulses from ETA II, and that the most intensely heated region occurred approximately 1 mm below the surface of the plate.

Therefore, the Monte Carlo code appears to correlate well with the HEEB processed steel sample in terms of predicting the peak dose, the depth-dose profile, and the overall distribution of energy in the processed sample. This good correlation between the experiments and the calculations indicates that the Monte Carlo code can be used to estimate the beam processing parameters, *i.e.*, beam diameter, beam energy, beam fluence, etc., for producing desired metallurgical modifications to steel. In addition, this computational method can be used as an inexpensive method for predicting the interaction of HEEBs with materials that have different thermophysical properties than steel, thus allowing processing parameter windows to be defined prior to performing the actual HEEB processing experiments.

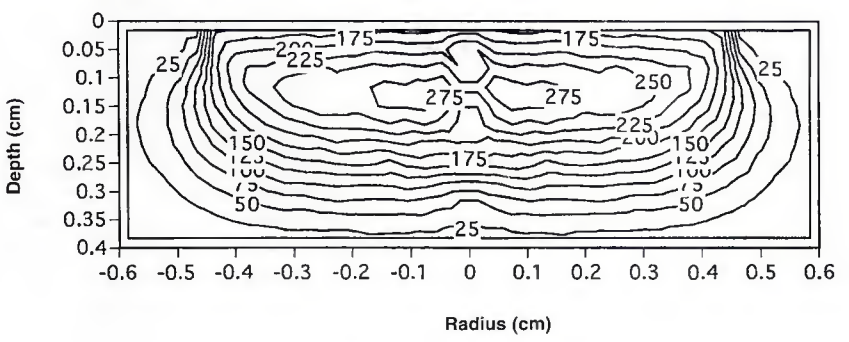

Fig. 16 — CYLTRAN Monte Carlo calculations of the energy deposition in O-1 tool steel for 1 pulse from a stationary 9-mm-diameter, 6-MeV beam operating at 1.25-kA/pulse. Contours are marked in J/g.

Table 1 — Thermophysical Properties of Iron

ρ (g/mm^3)	k (W/mmK)	Cp (J/gK)	α (mm^2/s)	$\Delta H_{\alpha-\gamma}$ (J/g)	$\Delta H_{\gamma-L}$ (J/g)	ΔH_{L-v} (J/g)
7.86×10^{-3}	0.047	0.486	12.3	15	247	6085

Table 3 — Total Dose Required for the Indicated Phase Transitions in 0.94%C Steel (J/g)

Dose to $T = T_{A3}$	Dose to austenitize	Dose to $T = T_L$	Dose to melt	Dose to $T = T_v$	Dose to vaporize
560	575	960	1207	2110	8195

Conclusions

1) The 6-MeV HEEB experiments on steel showed that the peak energy deposition occurs approximately 1 mm below the surface of the processed plate. This deep energy penetration allows HEEBs to be used for localized heating/annealing of steel to depths that cannot be accomplished by other localized heat sources.

2) The interaction of a stationary 6-MeV pulsed electron beam with plain carbon steel showed that a beam fluence of 21 J/mm^2 will transformation harden the steel without melting. At higher fluences, subsurface melting was observed at approximately 50 J/mm^2, subsurface vaporization was observed at 95 J/mm^2, and drilling was observed at fluences of 140 J/mm^2 and higher.

3) The depth of the HEEB transformed hardened zone extended nearly 2 mm below the surface of the steel plate. Processing was accomplished using either a stationary spot processing mode or by moving the beam at a scan rate of 0.4 m/s to produce strips of transformation hardened steel. In O-1 tool steel, the 6-MeV beam was used to heat treat strips of material to a hardness of 800 kg/mm^2, which is a factor of 3 to 4 increase over the hardness of the base material and is representative of the peak hardness for this material.

4) Localized heat treating at depth with a 6-MeV electron beam did not alter the macroscopic characteristics of the surface of the steel plate, therefore, localized heat treating of steel components can be performed in the final surface-finished condition. This avoids the large scale distortion that accompanies oil-quenching of bulk components, and avoids the formation of solidification-related defects that accompany localized heat treating processes that cause surface melting.

5) The 6-MeV electrons were shown to couple well with the steel at a glancing angle of 30 deg. Shallow angle coupling of the HEEB will enable nonflat components, such as gear teeth and turbine blades, to be hardened.

6) Monte Carlo calculations were used to simulate the HEEB/material interaction in steel, and the results of these calculations correlated well with experiments performed on the ETA II accelerator. These calculations can be used to predict the depth-dose profile and the location of the peak energy dose for a wide range of processing conditions and materials.

Acknowledgments

This work was performed under the auspices of the U.S. Department of Energy, Lawrence Livermore National Laboratory, under Contract No. W-7405-ENG-48.

The authors acknowledge the support of Don Prosnitz for providing access to the ETA II accelerator, Bob Kershaw for optical metallography, Mark Wall for transmission electron microscopy, Skip Fields and Scott Hulsey for operation of the electron beam accelerator, and Cliff Holmes and Don Hathaway for sample fixturing and preparation.

Table 2 — Coefficients for the Temperature-Dependent Heat Capacity of Iron

Parameter	Fe_{bcc}	Fe_{fcc}	Fe_L
a (J/gK)	0.664	0.438	0.749
b (J/gK^2)	0.110×10^{-3}	0.151×10^{-3}	—

References

1. Roth, M., and Cantello, M. 1985. Laser hardening of a 12%-Cr steel. *Proceedings of the Second International Conference on Lasers in Manufacturing*, IFS (Publications) Ltd, U.K., pp. 119–128.

2. Blaes, L.; Bauer, P.; Gonser, U.; and Kern, R. 1988. Depth profile of a laser irradiated steel. *Z. Metallk*, 79, p. 278.

3. Smith, A. C., Jr.; Nolting, E. E.; and Fawley, W. M. 1992. An overview of high energy electron beam science. Presented at High Energy Electron Beam Processing of Materials Conference, Cambridge, Mass.

4. Elmer, J. W;, Newton, M. A.; and Smith, A. C., Jr. 1993. Rapid thermal processing of steel using high energy electron beams. *The Laser and Electron Beam in Welding, Cutting and Surface Treatment State of the Art 1993*, Fifth Biannual Conference, Bakish Materials Corporation. pp. 91–104.

5. Chong, Y. P.; Deadrick, F. J.; Hirzel, D. G.; Kallman, J. S.; Lee, P.; Poulter, J. P. ; Rivera, W. E.; Stephan, P. L.; and Weir, J. Y. 1989. Optical Cerenkov measurements of emittance growth in the ATA beam under laser ion-guiding. Lawrence Livermore National Laboratory UCRL 99782, prepared for the 1989 Particle Accelerator Conference, Chicago, Ill, March 20–23.

6. *ASM Handbook*, Vol. 8, Ninth Edition, 1985. Mechanical testing, ASM International, Materials Park, Ohio, p. 110.

7. *Tool Steels*, 4th edition. 1980. G. A. Roberts and R. A. Carry, published by ASM International, Materials Park, Ohio.

8. *Heat Treater's Guide*. 1982. Standard practices and procedures for steel, published by ASM International, Materials Park, Ohio.

9. *Monte Carlo Transport of Electrons and Photons*. 1988. Editors T. M. Jenkins, W. R. Nelson, and A. Rindi, Plenum Press.

10. *Handbook of Chemistry and Physics*, 54th edition. CRC Press, 1974.

11. *Metallurgical Thermochemistry*, 5th edition, 1979. O. Kubaschewski and C. B. Alcock, published by Pergamon Press.